5th Australasian Congress on Applied Mechanics, ACAM 2007
10-12 December 2007, Brisbane, Australia

Title – X-Ray Imaging for the Observation of Mode I Fracture in Fibre Reinforced Concrete

Trevor N.S. Htut[1] **and Stephen J. Foster**[2]

[1]*School of Civil and Environmental Engineering, University of New South Wales, Sydney*
[2]*School of Civil and Environmental Engineering, University of New South Wales, Sydney*

Abstract: In this study X-ray imaging is used to investigate the mechanisms of fracture in fibre reinforced concrete. The investigation looks at the performance of discrete end-hooked fibres crossing a cracking plane at various angles and loaded normal to the plane. The angle of a fibre crossing a crack is found to be an important parameter in determining the mode of failure and bending of the fibres were observed up to approximately 5 mm into the matrix from the fibre exit point. The tests show a probability that some fibres pullout from longer embedded side under Mode I fracture. In the non-destructive observation procedure presented here, the internal actions of the fibres at the various stages of loading can be determined. X-Ray imaging is shown to be a valuable tool in understanding steel fibre-concrete behaviour.

Keywords: fibre pullout, fibre reinforced concrete, mode I fracture, x-ray.

1 Introduction

It is generally agreed that mechanical properties of quasi-brittle cement-based materials such as ductility, durability, energy absorption, fatigue, increased service life and toughness can be significantly improved by reinforcing with fibres [1, 2]. In general the resistance to crack propagation provided by the fibre depends on the mechanical properties of the matrix and of the fibres such as the type of fibre and/or geometry, fibre orientation and fibre length.

There is no easy method to measure bond stresses between fibres and a cementitious matrix. Fibre pullout tests have been used to determine average interfacial bond behaviour of fibre-matrix interface. In randomly orientated fibre reinforced concrete, few fibres are aligned in the direction of the applied load; instead, almost all fibres are lying at an angle to the loading direction. In such cases, fibres are subjected to a combination of shear, bending and tensile stresses [3]. Due to their inclination angles, fibres bend at the exit point and snubbing or spalling of the matrix at the exit point is expected for fibres at high inclination angles [4]. This can give a substantial reduction in pullout resistance [5]. In addition to snubbing of the matrix, hooked-ended fibres at high inclination angles are more likely to fracture due to high stress concentrations at the bending point (i.e. near the crack surface) [6, 7]. Space in this paper prohibits an extensive review of the literature on Mode I fracture of fibre reinforced cementitious composites, however, more information on the topic can be found in [8].

It has been a common assumption in the modelling of fibre reinforced concrete that that fibres pullout from the shorter embedded side [9]. This was shown not to be correct, however, in recent research using radiographic imaging in Mode II fracture [10, 11]. In that study, radiographic imaging was used to highlight the importance of the snubbing effect in Mode II fracture.

In this study, X-Ray imaging was used to view the internal mechanism that evolves during pullout of fibres under Mode I fracture. An experimental program of fibre pullout tests was carried out and X-Ray images were taken at regular intervals. The variables considered in this study were fibre inclination angle, fibre embedment length, different fibre combinations and the effect of aggregate.

2 Experimental Program

2.1 Introduction

The study consists of four groups of pullout tests, each of which have a different combination of fibres and/or cementitious matrix. In the first series, the influence of the angle of the fibre on the pullout behaviour was investigated and end-hooked fibres placed at angles of 0°, 15°, 30°, 45° and 60° to the loading direction. The second series of pullout experiments was conducted to assess the influence of the embedment length. In this series, fibres were embedded at embedment ratios (short-side:long-

side) of 1:2 and at angles of 0°, 30°, 45° and 60°. The remaining two series were aimed at assessing the influence of fibre combinations and effect of aggregate within the matrix. In these series the fibres were aligned at 0°, 30° and 60° to the crack surface. Three specimens were tested for each test condition, one of which was performed in combination with X-Ray imaging.

2.2 Materials and specimen preparation

Figure 1 shows the specimen dimensions and fibre arrangements for the fibre pullout experiments. The specimens were fabricated in two separate pours. The fibre inclination angle (θ) is measured from a horizontal line drawn normal to the interface of the two halves of the specimen. The thickness of the specimen was 30mm.

A single row of four fibres were clamped into position for the first pour using a specially fabricated steel fibre clamp placed on the side of the specimen selected for the second pour. On the following day the steel clamp was released and the second side of the specimen was cast. Special attention was given to cleaning the fibres with acetone solution before pouring of cementitious matrices.

The mortar mix used in the specimens was composed of kiln dried Sydney sand and general purpose Portland cement mixed in a sand and cement ratio of 3:1 and water-cement ratio of 0.4. No other additives were added in the mix design. The concrete mix used in the specimen has similar constituent materials but with a maximum 10mm Basalt aggregate added with a fine to coarse aggregate ratio of 0.9.

The deformed steel fibres used in the tests were high strength, end-hooked, Dramix cold drawn fibres produced by Bekaert (Belgium). The fibre dimension and material properties are given in Table 1.

Table 1. Properties of steel fibres

Fibre Type	Dramix® RC-65/35-BN	Dramix® RC-65/60-BN
Diameter, *d* (mm)	0.55	0.9
Length, *l* (mm)	35	60
Aspect Ratio, *l/d*	64	67
Tensile Strength (MPa)	1100	1000

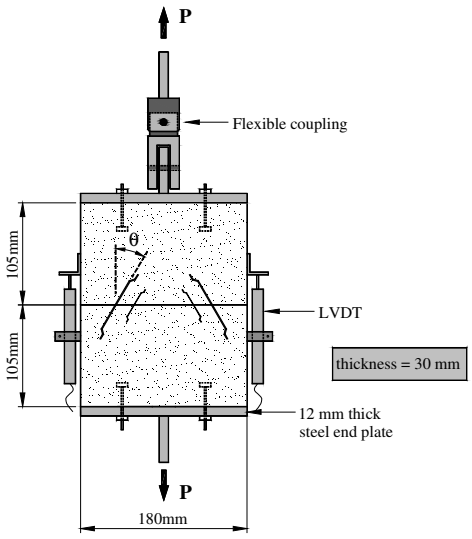

Figure 1. Testing arrangement

Details of the test specimens for the X-ray imaging are given in Table 2. The specimens are designated as NUTD±θXXX*a:b*Y where NUTD = "non-destructive uniaxial tension test on discrete fibres", ±θ is the fibre inclination angle, XXX is the fibre combination, and *a:b* is the ratio of the fibre embedment length on the short side relative to that of the long side and Y=A for specimens with aggregate. For example, NUTD±45Hyb1:2 is a non-destructive (X-ray imaging) test in uniaxial tension with an hybrid fibre consisting two of 35mm and two 60mm long hooked-ended fibres at an angle of 45°, a fibre embedment length of (l_e) of $l_e = 0.33l_f$ on the short side and $l_e = 0.67l_f$ on the long side, where l_f is the total length of the fibre (ie. short side embedment to long side embedment ratio is 1:2) and without aggregate.

Table 2. Specimen properties

Specimen	Fibre Combination	Fibre Inclination Angle, θ (degree)	Cylinder Strength (MPa)
NUTD±θHyb1:1	2 × (35mm and 60mm) long hooked-ended	0, 15, 30, 45 & 60	40 43
NUTD±θHyb1:2	2 × (35mm and 60mm) long hooked-ended	0, 30, 45 & 60	43 42
NUTD±θHooked1:1	4 × 60mm long hooked-ended	0, 30 & 60	33
NUTD±θHyb1:1A (with aggregate)	2 × (35mm and 60mm) long hooked-ended	0, 30 & 60	57

The specimens were cast horizontally in two stages into the moulds. The first stage involved casting a section on one side of the cracking plane, with the other half of the specimen blocked out and the fibres protected between two steel sandwich blocks (fibre clamp). The specimens were compacted on a vibrating table and then left to cure for 24 hours. After setting of the first half of the specimen, the steel clamps were removed from the second half of the specimen and the remaining half was cast. The completed specimens were then air cured for 24 hours to allow setting and then demoulded. Eight 200 mm high by 100 mm diameter cylinders and two 100 mm by 100 mm by 500 mm long rectangular prisms were cast with each half of the specimen for quality control.

After setting of the second half of the specimen, the specimens, cylinders and prisms were stripped and placed in the fog room for minimum of 28 days. After removal from the fog room all the specimens were stored in a laboratory environment until testing. The mean cylinder compressive strength at the time of testing is given in Table 2.

2.3 Testing arrangements

The testing arrangements are shown in Figure 1. The displacements in the direction of movement of the loading jacks were measured using two linear variable differential transducers (LVDTs), one placed on each side of the specimen. The displacement is taken as the average of the LVDT readings. Loading was conducted using displacement control at a rate of 0.2 mm per minute until the peak value was attained. The rate was then increased by a minimum of 0.1 mm per minute, with further rate increases introduced as necessary during the test. Each test specimen was loaded until fibres were either pullout completely from the section or fractured. Load and displacement readings were recorded at 1 second intervals.

3 Test results

Examples of the load versus crack opening displacement (COD) obtained from the tests are given in Figures 2 to 4 with the location of X-Ray image taken as indicated. The photo plate numbers are given as "P*x*" where *x* is the image number.

The X-ray negative images were converted into positives using digital scanner and the fibres within the matrix. While the fibres are clearly observed in the X-rays, they have been enhanced for reproduction in the figures of this paper. Two type of X-ray negative (Agfa NDT D4 & D7 films) were employed to obtained images within the matrix as well as images within the opened portion of the specimen. Complete images were obtained through subsequent overlaying of same images taken with different films.

In this study, together with results from the destructive tests a total of 47 tests were conducted. In total, observations on 188 fibres were recorded and a survey of the results is presented in Table 3 showing the mode of failure for the fibres.

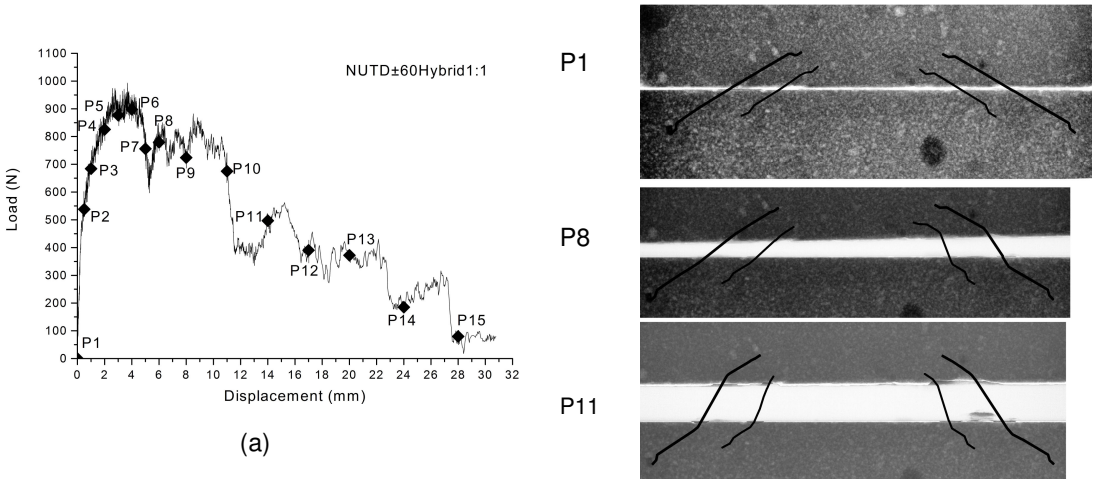

Figure 2. Specimen NUTD±60Hyb1:1: a) Load-displacement and b) X-Ray imaging.

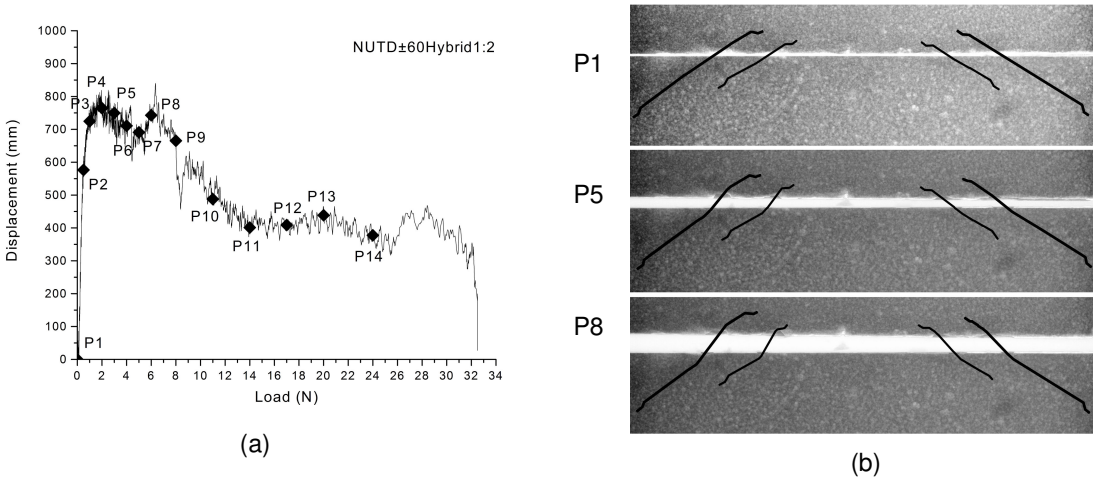

Figure 3. Specimen NUTD±60Hyb1:2: a) Load-displacement and b) X-Ray imaging.

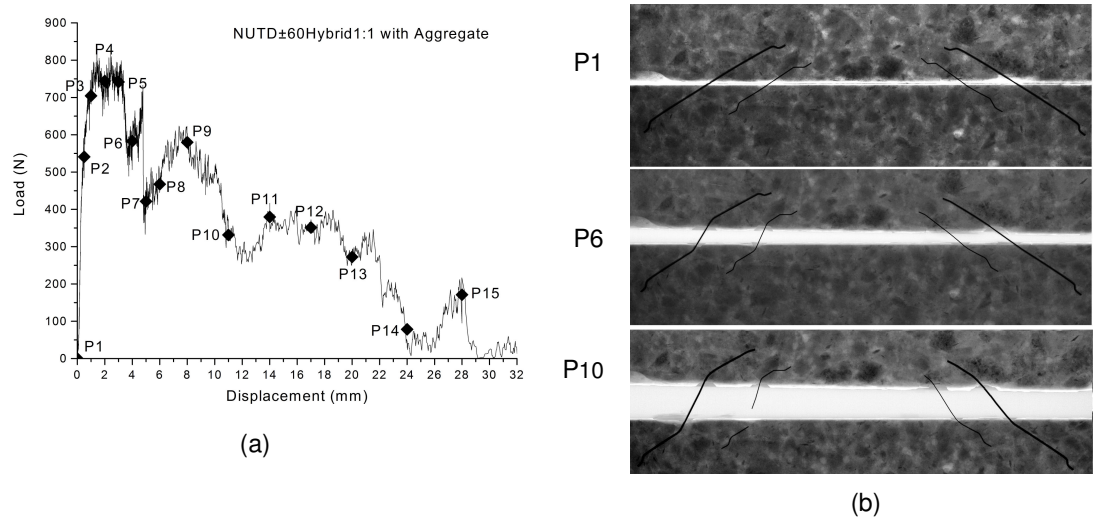

Figure 4. NUTD±60Hyb1:1A (with aggregate): a) Load-displacement and b) X-Ray imaging.

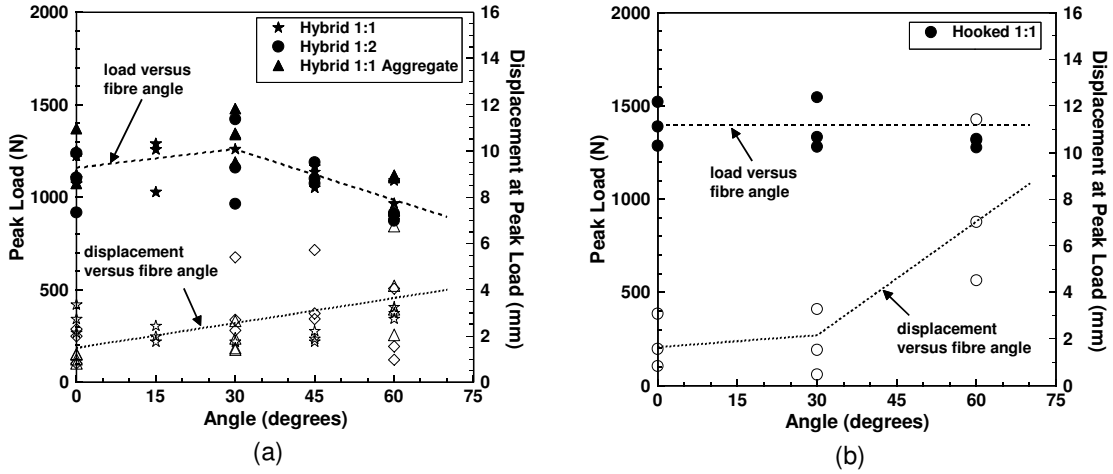

Figure 5. Peak loads (solid markers) and displacement at peak load (hollow markers) versus fibre angle for: a) hybrid fibre tests and b) single type hooked-ended fibre tests.

Table 3. Survey of discrete fibre failure

Specimen Group	Fracture	Total Pullout	Pullout from Short Embedment Side	Pullout from Long Embedment Side
DUTD±θHyb1:1	5	35	-	-
DUTD±θHyb1:2	2	30	23	7
DUTD±θHooked1:1	0	20	-	-
DUTD±θHyb1:1 with Aggregate	0	20	-	-
NUTD±θHyb1:1	0	16	-	-
NUTD±θHyb1:2	0	12	10	6
NUTD±θHooked1:1	2	22	-	-
NUTD±θHyb1:1 with Aggregate	3	21	-	-

4 Analysis of results

The fibre reinforced specimens failed in one of three modes: fibre pullout, fibre fracture or a combination of the two. Examining closely the images of specimen NUTD±60Hyb1:1 (Figure 2b) and NUTD±60Hyb1:1A (Figure 4b), it is seen that, for the fibres angled at 60°, bending of the fibres occurred deep within the matrix, up to 5 mm from the exit point.

In P6 of Figure 4a, at the peak load of 582 N all fibres were intact. However, shortly afterwards, it is observed that smaller fibre on the left fractured between P6 and P7, resulting in a 28% loss of load carrying capacity. Shortly afterwards, rotation at the top half of specimen allowed the load to be picked up by the stiffer half of the specimen where the fibres remained intact. Examining the X-ray images P6 and P10 in Figure 4b, the fibre fracture can be explained as a result of high stress concentration due to combined bending and tension.

Figure 5a shows that the embedment length on each side of the crack interface has only a little influence on the peak load. This is mainly due to the plastic deformation of the hooked end which contributes significantly to the maximum pullout load while the straight portion has only a small contribution.

Comparing Figure 5a and Figure 5b, it is seen that, for larger angles, the displacement at the peak load is lower for the hybrid fibre combination than for the fibres of the same (larger) size.

The survey data in Table 3 can be used to determine the probability that a fibre pullout from the longer embedded side. Based on the survey, it is observed that there is a 28% (13 fibres out of 46) probability that fibres pullout from longer embedded side for fibres with embedment ratio of 1:2. It is also observed that failure related to fibre fracture is more common for high fibre inclination angles. Further study is required on embedment lengths and snubbing effects for the development of rational behavioural models for describing Mode I fracture of fibre reinforced concrete.

5 Conclusions

X-ray imaging has shown the importance of the snubbing effect on the behaviour of fibre reinforced cement based matrices subject to Mode I fracture. For fibres at high inclination angles, bending of fibres during pullout was observed to occur within the matrix at up to 5 mm from the exit point. As has been previously observed by others, the snubbing effect dominates the behaviour of fibres at high inclination angles and the angle of a fibre crossing a crack is an important parameter in determining the mode of failure. Engagement of fibres is likely to occur earlier in hybrid fibre arrangements than non-hybrid arrangements of the larger fibre. It has been shown that there is a statistical chance that fibres pullout from the longer embedded side.

6 Acknowledgements

This study is funded via Australian Research Council (ARC) discovery grant DP0559742. The support of ARC is acknowledged with thanks.

References

[1] Gopalaratnam, V. S. & Shah, S. P. (1987) Tensile failure of steel fibre-reinforced mortar. Journal of Engineering Mechanics, Vol. 113, No. 5, 635-652.

[2] Guerrero, P. & Naaman, A. E. (2000) Effect of mortar fineness and adhesive agents on pullout response of steel fibres. ACI Materials Journal, Vol. 97, No. 1, 12-20.

[3] Bartos, P. J. M. & Duris, M. (1994) Inclined tensile strength of steel fibres in a cement-based composite. Composites, Vol. 25, No. 10, 945-952.

[4] Morton, J. & Groves, G. W. (1974) The cracking of composites consisting of discontinuous ductile fibres in a brittle matrix-effect of fibre orientation. Journal of Materials Science, Vol. 9, No. 9, 1436-1445.

[5] Naaman, A. E. & Shah, S. P. (1976) Pullout mechanism in steel fibre-reinforced concrete. Journal of the Structurel Division, Vol. 102, No. 8, 1537-1548.

[6] Naaman, A. E. & Najm, H. (1991) Bond-slip mechanisms of steel fibres in concrete. ACI Materials Journal (American Concrete Institute), Vol. 88, No. 2, 135-145.

[7] Robins, P., Austin, S. & Jones, P. (2002) Pullout behaviour of hooked steel fibres. Materials and Structures/Materiaux et Constructions, Vol. 35, No. 251, 434-442.

[8] Voo, J. Y. L. & Foster, S. J. (2004) Tensile-fracture of fibre-reinforced concrete: Variable engagement model IN DI PRISCO, M., FELICETTI, R. & PLIZZARI, G. A. (Eds.) Sixth RILEM Symposium on Fibre-Reinforced Concrete (FRC) - BEFIB 2004. Varenna, Italy, RILEM.

[9] Yip, M., (2005). "Irregular lattice simulation of cement composite materials and structures". Ph.D. Dissertation, University of California, Davis, United States -- California.

[10] Lee, G. G. & Foster, S. J., (2006). "Behaviour of steel fibre reinforced mortar in Shear II: Gamma Ray imaging". Report No. UNICIV R-445, School of Civil & Environmental Engineering, The University of New South Wales,

[11] Foster, S. J., Lee, G. G. & Htut, T. N. S. (2007) Radiographic imaging for the observation of Modes I and II fracture in fibre reinforced concrete. IN CARPINTERI, A., GAMBAROVA, P., FERRO, G. & PLIZZARI, G. A. (Eds.) The 6th International Conference on Fracture Mechanics of Concrete and Concrete Structures. Catania, Italy, Taylor & Francis.